IOPscience iopscience.iop.org

Home Search Collections Journals About Contact us My IOPscience

The characteristics and nature of planar defects in $Y_2Cu_2O_5$ and $Y_{2-x}Ca_xCu_2O_5$ with x = 0.05, 0.1, 0.2 and 0.4

This article has been downloaded from IOPscience. Please scroll down to see the full text article.

1998 J. Phys.: Condens. Matter 10 3497

(http://iopscience.iop.org/0953-8984/10/16/004)

View the table of contents for this issue, or go to the journal homepage for more

Download details:
IP Address: 171.66.16.209
The article was downloaded on 14/05/2010 at 12:58

Please note that terms and conditions apply.

J. Phys.: Condens. Matter **10** (1998) 3497–3507. Printed in the UK PII: S0953-8984(98)90458-1

The characteristics and nature of planar defects in $Y_2Cu_2O_5$ and $Y_{2-x}Ca_xCu_2O_5$ with $x = 0.05$, 0.1, 0.2 and 0.4

C N Feng† and D R Lovett‡

Department of Physics, University of Essex, Colchester CO4 3SQ, UK

Received 30 December 1997

Abstract. Planar defects found in $Y_2Cu_2O_5$ have been studied in detail. These planar defects are parallel to the $\boldsymbol{a}$–$\boldsymbol{b}$ plane with the displacement vector $\boldsymbol{R} = \frac{1}{2}[100]$. They arise from the movement of oxygen atoms within the structure. The dependence of the density of planar defects within $Y_2Cu_2O_5$ has also been studied by varying the amount of the dopant Ca, i.e. $Y_{2-x}Ca_xCu_2O_5$ with $x = 0.05$, 0.1, 0.2 and 0.4. There is no direct relationship between the density of the planar defects and the concentration of Ca.

1. Introduction

$Y_2Cu_2O_5$ is a semiconductor material. It has become of interest as it is one of the second phases of several high-T_C superconductor materials.

The crystal structure of $Y_2Cu_2O_5$ has been studied by means of x-ray diffraction (Kimizuka *et al* 1982, Lambert and Eysel 1986), powder neutron diffraction (Fjellvag *et al* 1988) and transmission electron microscopy (Baba-Kishi *et al* 1990). It has been confirmed by several groups that the crystal structure of $Y_2Cu_2O_5$ is isostructural with $Ho_2Cu_2O_5$ (Fjellvag *et al* 1988, Famery and Queyroux 1989).

Single crystals of $Y_2Cu_2O_5$ were not grown until 1994 when this was achieved by the flux method (Imanaka *et al* 1994). The specimens of $Y_2Cu_2O_5$ studied by Famery and Queyroux (1989) and Baba-Kishi *et al* (1990) were prepared as a secondary phase in the preparation of $YBa_2Cu_3O_{7-y}$. The specimens studied by Fjellvag *et al* (1988) and Jang *et al* (1994) were single-phase polycrystalline and single crystals of $Y_2Cu_2O_5$ respectively. In spite of the different methods for preparing the specimens, the lattice parameters and the space group reported by several research groups are similar. However, different authors have different conventions for the crystallographic orientation of the axes. If we unify their results by applying a suitable rotation matrix, we can find that the unit cell of $Y_2Cu_2O_5$ which has a space group $Pna2_1$ is an orthorhombic structure with lattice parameters $a = 1.0796$ nm, $b = 0.3494$ nm and $c = 1.2457$ nm. We choose the space group $Pna2_1$ here as it is the standard space group (Henry and Lonsdale 1965).

Planar defects within $Y_2Cu_2O_5$ were first reported by Baba-Kishi *et al* (1990). The displacement vector for the planar defects was $\boldsymbol{R} = \frac{1}{2}[014]$ (space group $P2_1nb$). Baba-Kishi *et al* inferred that these planar defects were caused by Ba/Sc atoms which do not

† Current address: 168 Materials Research Laboratory, The Pennsylvania State University, University Park, PA 16802, USA.

‡ Responsible for communications. Email address: loved@essex.ac.uk

0953-8984/98/163497+11$19.50 © 1998 IOP Publishing Ltd

react with $Y_2Cu_2O_5$ to form solid solution. Since then, there have been no further reports on the planar defects.

The purpose of this paper is to re-examine the displacement vector of the planar defects found in single-phase $Y_2Cu_2O_5$. In addition, these planar defects as found in the $Y_2Cu_2O_5$ phase within specimens $Y_{2-x}Ca_xCu_2O_5$ with $x = 0.05$, 0.1, 0.2 and 0.4 are studied. The dependence of the density of the planar defects within these materials is also presented.

2. Experiment

The ceramic bulk samples of $Y_2Cu_2O_5$ and $Y_{2-x}Ca_xCu_2O_5$ with $x = 0.05$, 0.1, 0.2 and 0.4 used in this study were supplied by Dr K Z Baba-Kishi. These samples had been sintered previously at 1050 °C for 6 hours and cooled at a rate of 50 °C h^{-1}. Samples for transmission electron microscopy were thinned first by mechanical polishing followed by argon-atom beam bombardment. Electron microscopy was carried out using a transmission electron microscope, JEM 200CX at a voltage of 200 kV.

Before the determination of the displacement vector for the planar defects, the lattice parameters of the crystal structure were checked by reconstructing the reciprocal lattice cell. Photographs of the planar defects were taken under two-beam and many-beam conditions. The displacement vector was determined by the criteria of the visibility of the planar defects, i.e. $\boldsymbol{g} \cdot \boldsymbol{R} = 0$.

3. Results and discussion

3.1. Lattice parameters

A series of electron diffraction patterns was obtained from the $Y_2Cu_2O_5$ specimen. Figure 1 is part of a series of electron diffraction patterns with low-order zone axes. These diffraction patterns were obtained by tilting the $Y_2Cu_2O_5$ crystal around an axis which is indicated by $\boldsymbol{R}_3$ as shown in the photographs. The measured angles between the zone axes represented by each electron diffraction pattern in figure 1 are $\angle AB = 17.8^\circ$, $\angle BC = 14.6^\circ$, $\angle CD = 11.2^\circ$, $\angle DE = 8.2^\circ$ and $\angle EF = 38.5^\circ$, where A to F represent the labels of the photographs in figure 1. Specimens $Y_{2-x}Ca_xCu_2O_5$ with $x = 0.05$, 0.1, 0.2 and 0.4 contain two crystalline phases. Electron diffraction patterns obtained from $Y_2Cu_2O_5$ phase within these specimens show the same characteristics as those in figure 1.

To confirm the geometrical relation between each diffraction pattern, we draw the horizontal cross-sectional view of the diffraction patterns of figure 1 as shown in figure 2. $\boldsymbol{R}_A$ to $\boldsymbol{R}_F$ are the reciprocal lattice vectors from the central spot of the diffraction patterns to the first diffraction spot at the right-hand side as indicated in figure 1. $\boldsymbol{R}_3$ is now perpendicular to the plane of the paper. From this diagram (figure 2), we can see that the projections of $\boldsymbol{R}_B$, $\boldsymbol{R}_C$, $\boldsymbol{R}_D$, and $\boldsymbol{R}_E$ along $\boldsymbol{R}_A$ are equal to $\frac{1}{2}|\boldsymbol{R}_A|$, and the projection of $\boldsymbol{R}_C$ along $\boldsymbol{R}_F$ equals $|\boldsymbol{R}_F|$. These projections indicate that the data we obtained fulfill the appropriate geometrical relations.

Choosing the rectangles formed by $\boldsymbol{R}_3 - \boldsymbol{R}_A$, $\boldsymbol{R}_3 - \boldsymbol{R}_B$ and $\boldsymbol{R}_3 - \boldsymbol{R}_F$ where $\boldsymbol{R}_A$, $\boldsymbol{R}_B$, $\boldsymbol{R}_F$ and $\boldsymbol{R}_3$ are the vectors as shown in figure 1, we construct the reciprocal lattice cell as shown in figure 3. The reciprocal lattice cell in figure 3 shows no body- or face-centred cell. Thus, it is a primitive cell. The lattice cell in real space is, then, primitive. By assigning the Miller indices as shown in figure 3, the lattice parameters are $a = 1.08$ nm, $b = 0.35$ nm and $c = 1.23$ nm. These values are compatible with the values reported by other authors (e.g. by Kimizuka *et al* 1982, Lambert and Eysel 1986, Fjellvag *et al* 1988 and Baba-Kishi

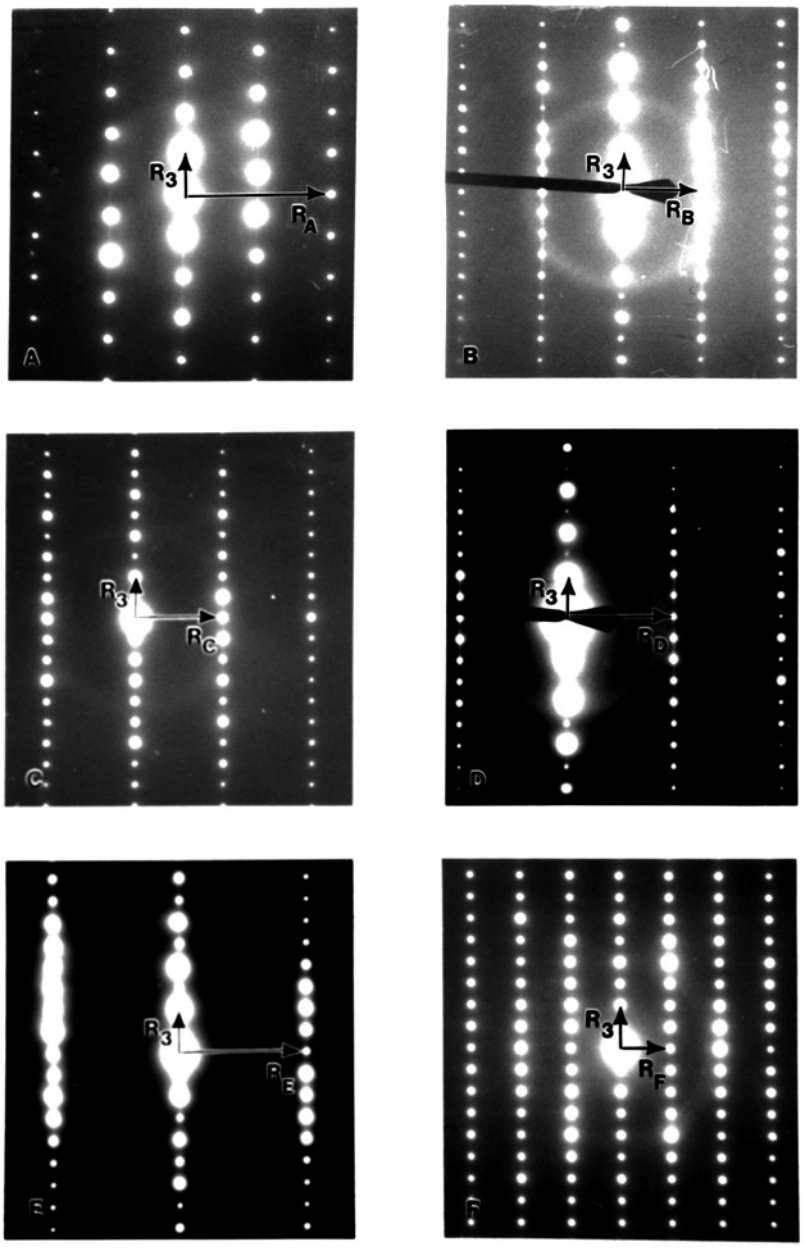

Figure 1. Part of the series of electron diffraction patterns obtained from $Y_2Cu_2O_5$ with zone axes along (A) [100], (B) [110], (C) [120], (D) [130], (E) [140] and (F) [010] respectively.

et al 1990), i.e. $a = 1.0796$ nm, $b = 0.3494$ nm and $c = 1.2457$ nm. According to the diffraction conditions of the diffracted beams, the space group for the crystal structure is concluded to be $Pna2_1$. The zone axes of the electron diffraction patterns in figure 1 are then [100], [110], [120], [130], [140] and [010] respectively.

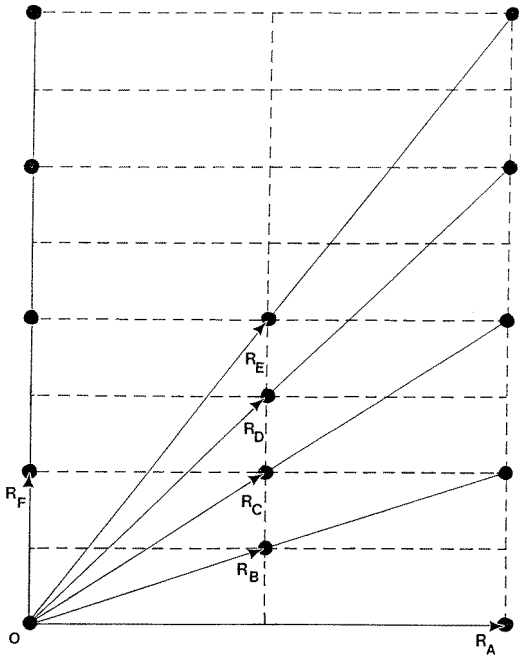

Figure 2. Horizontal cross-sectional view of the electron diffraction patterns in figure 1. $\boldsymbol{R}_A$ to $\boldsymbol{R}_F$ are the vectors indicated in figure 1.

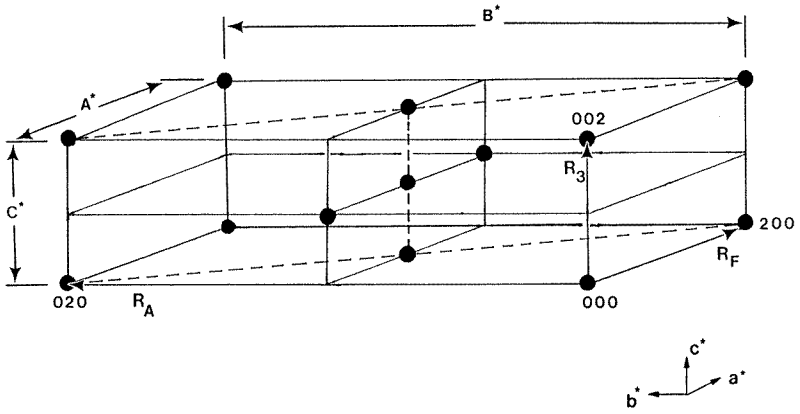

Figure 3. Diagram showing the reciprocal lattice cell of $Y_2Cu_2O_5$ constructed by using the rectangles formed by $\boldsymbol{R}_3 - \boldsymbol{R}_A$, $\boldsymbol{R}_3 - \boldsymbol{R}_B$ and $\boldsymbol{R}_3 - \boldsymbol{R}_F$ as shown in figure 1.

3.2. Electron micrographs

In figures 1(B) and (D), we can see there are streaks along the $\boldsymbol{c}^*$ direction. Their presence indicates that there are defects within this crystal (Reimer 1984). Figure 4 shows low-magnification lattice images of the same crystal within the sample $Y_2Cu_2O_5$ with the electron beam along the [100], [110], [120], [130] and [140] directions respectively. They have a common axis of rotation, the $\boldsymbol{c}$ axis. In these photographs, we can see some fringes with

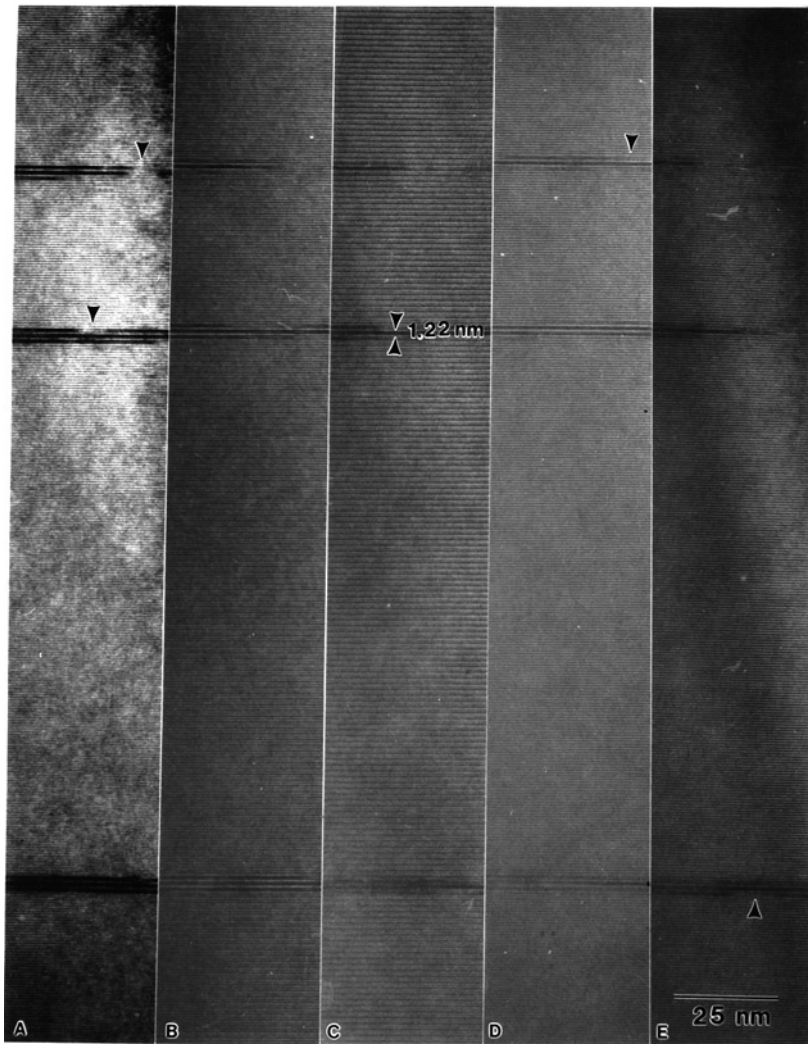

Figure 4. Low-magnification lattice images of the same crystal with the electron beam along the (A) [100], (B) [110], (C) [120], (D) [130] and (E) [140] directions respectively.

weaker intensity. These arise because of the interference of the electron beams which are out of phase. The normal to these fringes is along the $\boldsymbol{c}^*$ direction. Thus the planar defects are parallel to the $\boldsymbol{a}$–$\boldsymbol{b}$ plane.

Fringes which indicate the location of planar defects show no continuity through the crystal as indicated by arrows in the photographs. This is probably because of the local variation of the crystal structure. The gap between two perfect regions is about 1.22 nm which is approximately the value of the c parameter. The spacing of fringes within perfect regions in each photograph also shows some differences, i.e. the spacing of fringes in figures 4(A), (D) and (E) are equally separated, while they look paired in figures 4(B) and (C). This is because of the difficulty of obtaining precise focusing.

In certain cases, we have been able to obtain higher-resolution lattice images. One of these is shown in figure 5 with the electron beam along the [010] direction. We can see that

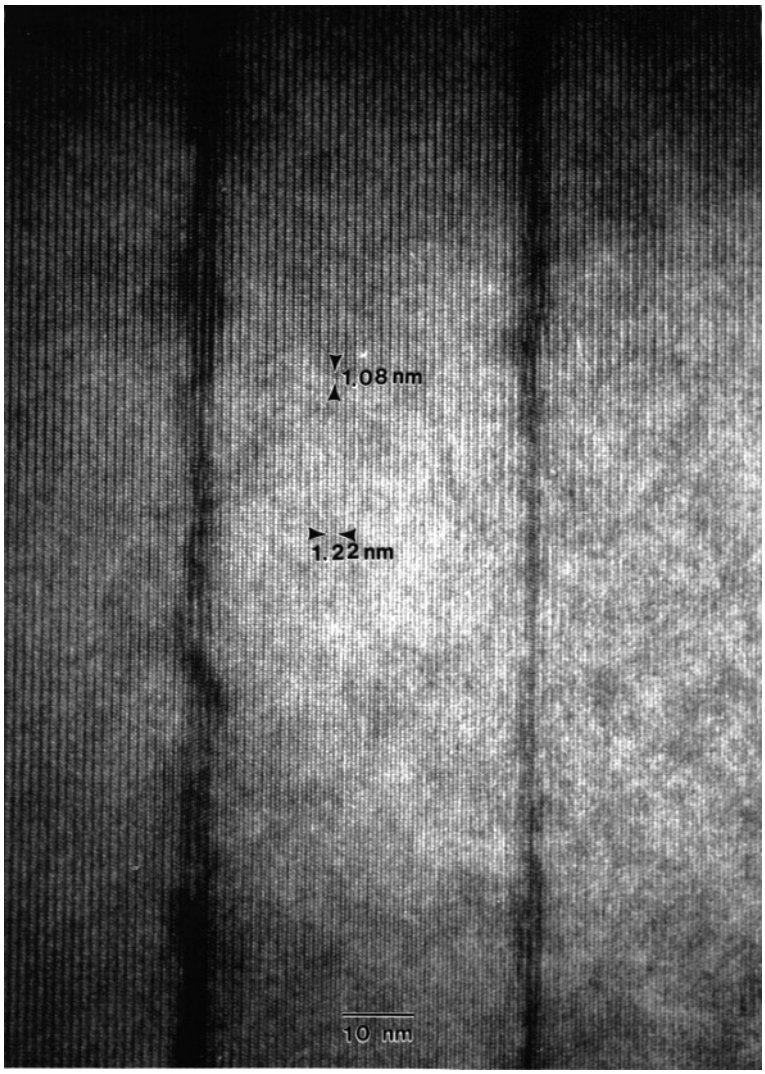

Figure 5. Higher-resolution lattice image with electron beam along the [010] direction.

the bright spots are regularly distributed within the unfaulted part of the crystal. However, their distribution is altered within the faulted regions of the crystal. Some spots within the faulted region are not clearly separated and thus form lines tilted to the lines in the unfaulted structure. In addition, some columns of spots which extend from the unfaulted part into the faulted region disappear. These situations occur because electrons which pass through the faulted region are diffracted differently from those which go through the perfect part. The width of the faulted area equals the value of the *c* parameter. This indicates that the fault occurs within a unit cell.

Figure 6 shows the dark-field images of the planar defects (dark lines in the photographs) taken from different crystallites within the sample $Y_2Cu_2O_5$. These dark-field images were taken along the [100] direction under the many-beam condition. Figure 7 also shows the dark-field images of the planar defects within a crystal with the electron beam along the

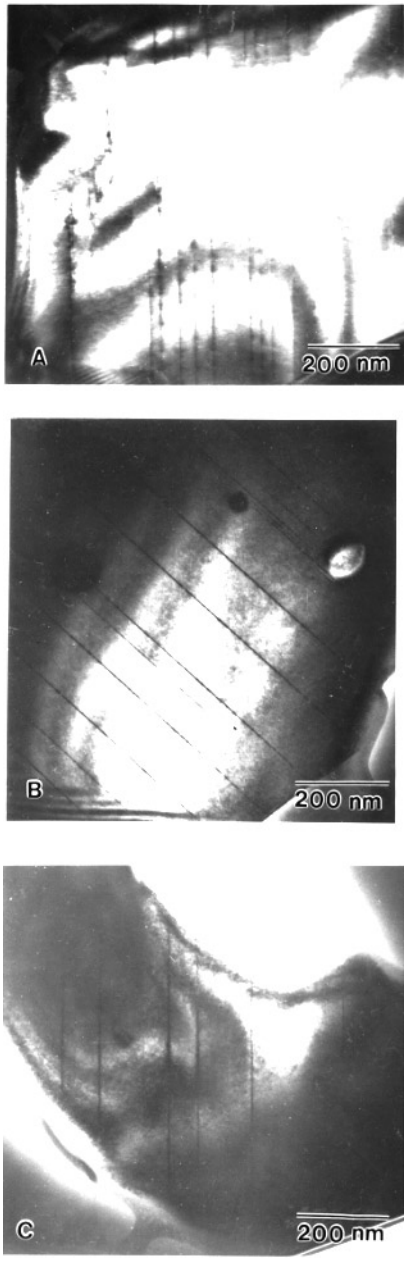

Figure 6. The dark-field images of the planar defects (dark lines in the photographs) under the many-beam condition. These dark-field images from different crystals were taken with the electron beam along [100].

[100], [110], [120] and [130] directions. From these photographs, we can see that the orientation of these defects follows a specific crystallographic orientation. They separate the whole crystal into parallel lamellae. In addition, their distribution does not form any periodicity. The density of the defects also shows no identified dependence, i.e. their

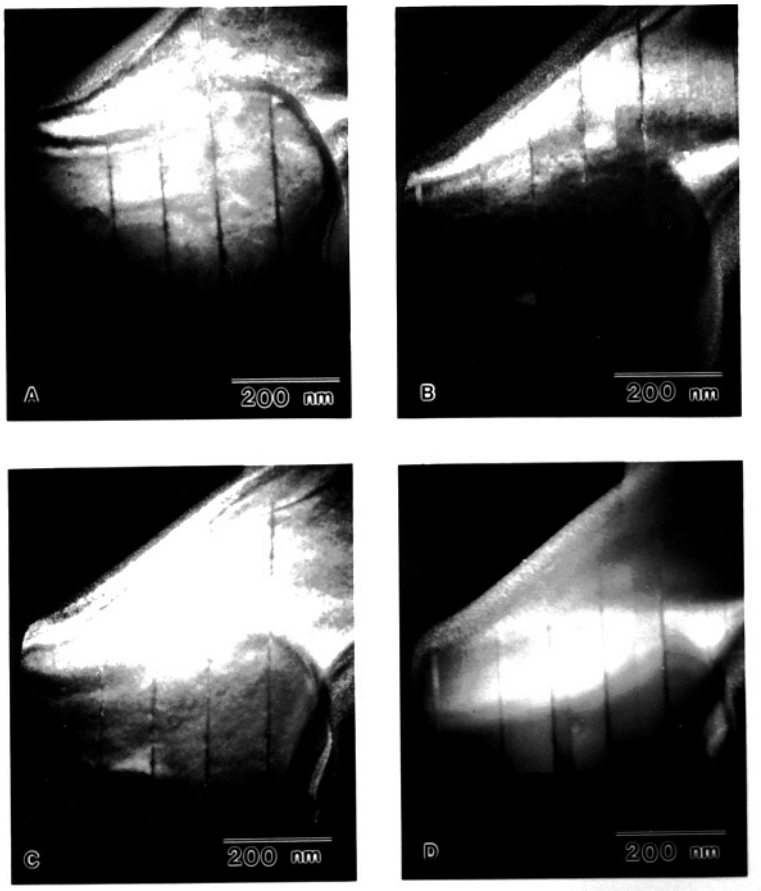

Figure 7. The dark-field images of the planar defects within a crystal with the electron beam along the [100], [110], [120] and [130] directions.

densities vary from crystal to crystal.

Figure 8 shows the electron micrographs obtained from the samples $Y_{1.95}Ca_{0.05}Cu_2O_5$, $Y_{1.9}Ca_{0.1}Cu_2O_5$, $Y_{1.8}Ca_{0.2}Cu_2O_5$ and $Y_{1.6}Ca_{0.4}Cu_2O_5$. We can see from figures 7 and 8 that there is no direct relationship between the density of the planar defects within $Y_2Cu_2O_5$ phase and the concentration of Ca.

3.3. Determination of displacement vector

An important parameter to describe the characteristic of planar defects is the displacement vector $\boldsymbol{R}$. This parameter can be calculated using the formula $\boldsymbol{g} \cdot \boldsymbol{R} = n$, where n is zero or integer.

We have tried to achieve the two-beam condition on the diffracted beams, $\bar{1}10$, $\bar{2}02$, $\bar{1}1\bar{2}$, $\bar{2}10$ and $\bar{4}12$. The image of the defects can be seen in the dark-field images obtained by selecting the diffracted beams $\bar{1}10$ and $\bar{1}1\bar{2}$, but not those from $\bar{2}10$, $\bar{4}12$ and $\bar{2}02$. So we use the three indices, $\bar{2}10$, $\bar{4}12$ and $\bar{2}02$, to calculate the displacement vector $\boldsymbol{R}$.

From $\boldsymbol{g} \cdot \boldsymbol{R} = n$, we let the displacement vector $\boldsymbol{R}$ be $[xyz]$ and substitute $\bar{2}10$, $\bar{4}12$

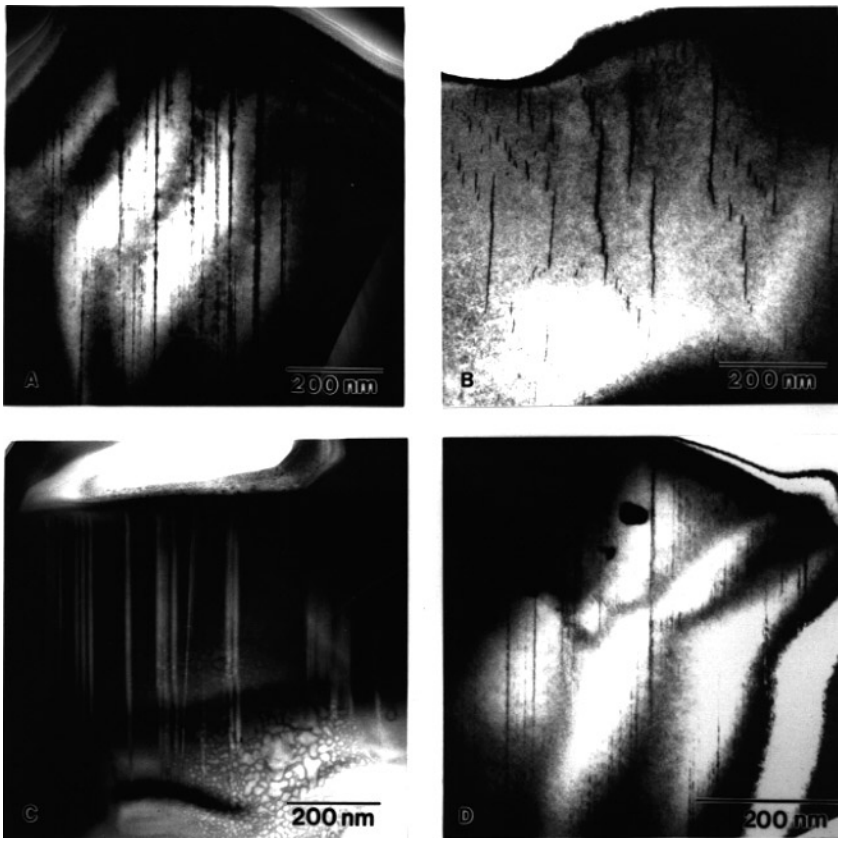

Figure 8. The electron micrographs of the samples (A) $Y_{1.95}Ca_{0.05}Cu_2O_5$, (B) $Y_{1.9}Ca_{0.1}Cu_2O_5$, (C) $Y_{1.8}Ca_{0.2}Cu_2O_5$ and (D) $Y_{1.6}Ca_{0.4}Cu_2O_5$.

and 202 into $\boldsymbol{g}$ respectively. We obtain the following equations:

$$\begin{aligned}
\boldsymbol{g}_1 \cdot \boldsymbol{R} &= [\,h_1 \quad k_1 \quad l_1\,] \cdot [\,x \quad y \quad z\,] = [\,\bar{2} \quad 1 \quad 0\,] \cdot [\,x \quad y \quad z\,] = \alpha \\
\boldsymbol{g}_2 \cdot \boldsymbol{R} &= [\,h_2 \quad k_2 \quad l_2\,] \cdot [\,x \quad y \quad z\,] = [\,\bar{4} \quad 1 \quad 2\,] \cdot [\,x \quad y \quad z\,] = \beta \\
\boldsymbol{g}_3 \cdot \boldsymbol{R} &= [\,h_3 \quad k_3 \quad l_3\,] \cdot [\,x \quad y \quad z\,] = [\,2 \quad 0 \quad 2\,] \cdot [\,x \quad y \quad z\,] = \gamma
\end{aligned}$$

where α, β and γ are integers. Solving the equations above, we have

$$x = \tfrac{1}{4}(\alpha - \beta + \gamma) \qquad y = \tfrac{1}{2}(3\alpha - \beta + \gamma) \qquad z = \tfrac{1}{4}(-\alpha + \beta + \gamma).$$

From the lattice image in figure 4, we know that $\boldsymbol{R}$ is parallel to the $\boldsymbol{a}$–$\boldsymbol{b}$ plane, i.e. $\boldsymbol{R} \cdot [\,0 \quad 0 \quad l\,] = 0$. So

$$[\,x \quad y \quad z\,] \cdot [\,0 \quad 0 \quad l\,] = 0 \quad \Rightarrow \qquad z = 0.$$

By substituting β and γ in turn with odd or even numbers, the results are summarized in table 1. We can see that the displacement vector is $\frac{1}{2}[100]$.

As an example, if we let $\beta = 0$ and $\gamma = 1$, so that $\alpha = 1$, the resultant displacement vector $\boldsymbol{R}$ is $\frac{1}{2}[140]$ which is the same as the displacement vector reported by Baba-Kishi *et al* (1990). If we decompose $\boldsymbol{R}$ into $\frac{1}{2}[100] + [010]$, the primitive displacement vector $\frac{1}{2}[100]$ is obtained.

Table 1. Results of possible displacement vectors under different combinations of β and γ.

β	γ	Result ($\boldsymbol{R} = [\frac{1}{2}\gamma\ \beta + 2\gamma\ 0]$)
even ($2n$)	even ($2m$)	$[m\ 2n + 4m\ 0]$
odd ($2n + 1$)	even ($2m$)	$[m\ 2n + 4m + 1\ 0]$
even ($2n$)	odd ($2m + 1$)	$\frac{1}{2}[2m + 1\ 4(n + 2m + 1)\ 0] = [m\ 2n + 4m + 2\ 0] + \frac{1}{2}[100]$
odd ($2n + 1$)	odd ($2m + 1$)	$\frac{1}{2}[2m + 1\ 2(2n + 4m + 3)\ 0] = [m\ 2n + 4m + 3\ 0] + \frac{1}{2}[100]$

3.4. Model of the planar defects

According to the discussion above, the fault is within a unit cell and parallel to the $\boldsymbol{a}$–$\boldsymbol{b}$ plane. The displacement vector equals 1/2[100]. Thus the fault is formed by a shear along the [100] direction with a displacement of half the a parameter.

Table 2. A complete list of atomic positions of $Y_2Cu_2O_5$ structure.

Atom	x	y	z	x	y	z	x	y	z	x	y	z
Y1	0.206 70	0.2310	0.0000	0.7933	0.7690	0.5000	0.7067	0.2690	0.0000	0.2933	0.7310	0.5000
Y2	0.040 60	0.2320	0.3290	0.9594	0.7680	0.8290	0.5406	0.2680	0.3290	0.4594	0.7320	0.8290
Cu1	0.990 90	0.6560	0.1123	0.0091	0.3440	0.6123	0.4909	0.8440	0.1123	0.5091	0.1560	0.6123
Cu2	0.206 20	0.6740	0.2151	0.7938	0.3260	0.7151	0.7062	0.8260	0.2151	0.2938	0.1740	0.7151
O1	0.176 10	0.7230	0.3487	0.8239	0.2770	0.8487	0.6761	0.7770	0.3487	0.3239	0.2230	0.8487
O2	0.326 20	0.7330	0.0665	0.6738	0.2670	0.5665	0.8262	0.7670	0.0665	0.1738	0.2330	0.5665
O3	0.123 00	0.3140	0.1650	0.8770	0.6860	0.6650	0.6230	0.1860	0.1650	0.3770	0.8140	0.6650
O4	0.431 00	0.7810	0.2630	0.5690	0.2190	0.7630	0.9310	0.7190	0.2630	0.0690	0.2810	0.7630
O5	0.424 10	0.2360	0.4700	0.5759	0.7640	0.9700	0.9241	0.2640	0.4700	0.0759	0.7360	0.9700

A complete list of the atomic positions of $Y_2Cu_2O_5$ is given in table 2. A shift along the [100] direction with displacement $1/2a$ means that $1/2a$ must be added to the x coordinate of all the atoms whilst keeping their y and z coordinates unchanged. Thus, the Y atom at (0.2067, 0.231, 0) becomes (0.7067, 0.231, 0) after the displacement, i.e. (0.2067, 0.231, 0) + (0.5, 0, 0) = (0.7067, 0.231, 0). If we compare the Y atom at (0.7067, 0.269, 0) before the displacement with the Y atom at (0.7067, 0.231, 0) after the displacement, we can see that this displacement can be produced effectively by shifting the Y atom at (0.7067, 0.269, 0) to (0.7067, 0.231, 0) along the $\boldsymbol{b}$ direction, i.e. (0.7067, 0.269, 0) − (0, 0.038, 0) = (0.7067, 0.231, 0). This leads to the idea that the same displacement can be achieved by shifting the Y atom from (0.2067, 0.231, 0) to (0.2067, 0.269, 0), and similarly from (0.7067, 0.269, 0) to (0.7067, 0.231, 0). The displacement is only $0.038b$ along the [010] direction. This displacement needs less energy than shifting the atoms $1/2a$ along the [100] direction. A further check is therefore made and it is found that the shifts of the oxygen atoms at (0.4241, 0.236, 0.47), (0.9241, 0.264, 0.47), (0.5759, 0.765, 0.97) and (0.0759, 0.736, 0.97) are $0.028b$ along the [010] direction. The displacement of oxygen atoms is the smallest displacement possible of the alternatives to produce the faulted structure. The displacements do not need very much energy as there is only a small disturbance of the Y–O bonds.

Because of the symmetry, the shifts of atoms along the $\boldsymbol{b}$ direction produce no change under transmission electron microscopy when inspecting the structure along the $\boldsymbol{a}$ direction. However, the displacements along the $\boldsymbol{a}$ direction arising from the shifts can be seen under transmission electron microscopy when inspection is along the $\boldsymbol{b}$ direction.

Thus in our model, the defects found in $Y_2Cu_2O_5$ are not caused by a deficiency of oxygen. They arise from the movement of oxygen atoms (stacking faults). The appearance of a high density of defects in the specimens ($YBa_2Cu_3O_7$ and $YSr_2Cu_3O_7$) used by Baba-Kishi *et al* (1990) arose because the barium and the strontium do not actively interact with $Y_2Cu_2O_5$ to form a solid solution. Some of the barium and strontium migrate from the pure phase towards grain boundaries and force the oxygen atoms to shift from their original position. Consequently, serious defects are observed. These serious defects and the associated variation of electron density cause, according to our model, the stronger intensity of the streaks in the diffraction patterns of Baba-Kishi *et al* (1990).

4. Conclusions

The crystal structure of $Y_2Cu_2O_5$ has been confirmed by transmission electron microscopy. It is an orthorhombic cell with lattice parameters $a = 1.08 \pm 0.02$ nm, $b = 0.35 \pm 0.03$ nm and $c = 1.23 \pm 0.02$ nm, space group $Pna2_1$. The volume of the cell is 0.46 ± 0.06 nm^3. The lattice parameters we obtain are very close to other quoted results.

The planar defects in $Y_2Cu_2O_5$ are parallel to the $\boldsymbol{a}$–$\boldsymbol{b}$ plane with displacement vector $\boldsymbol{R} = \frac{1}{2}[100]$. A model for the planar defects has been proposed. These defects come from the disturbance of the Y–O bond during the formation of the crystal, i.e. from a stacking fault.

From the electron micrographs, the density of the planar defects within $Y_2Cu_2O_5$ phase has no direct relationship with the concentration of Ca.

Acknowledgments

The authors wish to thank Professor D J Barber and Dr Z Huang for useful discussions. One of the authors (CNF) acknowledges an Overseas Research Student Award from the CVCP.

References

Baba-Kishi K Z, Camps R A and Thomas P A 1990 *J. Phys.: Condens. Matter* **2** 5085–95
Fjellvag H, Karen P and Kjekshus A 1988 *Acta Chem. Scand.* A **42** 144–7
Hirotsu Y, Tomioka O, Ohkubo T, Yamamoto N, Nakamura Y, Nagakura S, Komatsu T and Matsushita K 1988 *Japan. J. Appl. Phys.* **27** L1869–72
Imanaka N, Adachi G, Dabkowska H, Dakkowski A and Greedan J E 1994 *J. Cryst. Growth* **141** 150–2
Jang W J, Hasegawa M, Zhao T R, Takei H, Tamura M and Kinoshita M 1994 *J. Cryst. Growth* **141** 153–8
Kimizuka N, Takayama E and Horiuchi S 1982 *J. Solid State Chem.* **42** 322–4
Lambert U and Eysel W 1986 *Powder Diffraction* **1** 45–50
Matsui Y, Maeda H, Tanaka Y and Horiuchi S 1988 *Japan. J. Appl. Phys.* **27** L372–5
Onoda M, Yamamoto A, Takayama-Muromachi E and Takekawa S 1988 *Japan. J. Appl. Phys.* **27** L833–6
Reimer L 1984 *Transmission Electron Microscopy* (Berlin: Springer)
Shaw T M, Shivashankar S A, La Placa S J, Cuomo J J, McGuire T R, Roy R A, Kelleher K H and Yee D S 1988 *Phys. Rev.* B **37** 9856–8